JOURNAL OF MATERIALS SCIENCE 29 (1994) 5455–5461

Sintering studies on submicrometre-sized Y–Ba–Cu-oxide powder

L. C. PATHAK, S. K. MISHRA, P. G. MUKUNDA*, M. M. GODKHINDI*, D. BHATTACHARYA, K. L. CHOPRA
*Materials Science Centre, and *Department of Metallurgical Engineering, Indian Institute of Technology, Kharagpur, India 721 302*

The isothermal sintering behaviour of submicrometre-sized (< 50 nm) powders of single-phase $YBa_2Cu_3O_x$ (123) and unreacted stoichiometric mixture of submicrometre-sized (< 50 nm) powders of $BaCO_3$, Y_2O_3 and CuO (which on calcination at 1173 K gives $YBa_2Cu_3O_x$) was investigated through dilatometry under different sintering atmospheres. The sintering rate of the powder compacts was impeded by the presence of oxygen. The activation energies, Q, of sintering were determined to be 1218 kJ mol^{-1} in argon, 1593 kJ mol^{-1} in air and 2142 kJ mol^{-1} in oxygen. A decrease in the apparent sintered density with increasing oxygen partial pressure was also observed. X-ray diffraction and thermal analyses (thermogravimetry and differential thermal analysis) showed no reaction during sintering of the single-phase product. Pellets fabricated from uncalcined powder exhibit two stages of sintering, one between 1073 and 1173 K having an activation energy $Q = 627$ kJ mol^{-1}, and a second one above 1173 K with $Q = 383.7$ kJ mol^{-1}. A.c. susceptibility, resistivity and critical current density were determined as a function of the temperature of the sintered samples.

1. Introduction

There have been few reports on the study of the sintering characteristics of $YBa_2Cu_3O_x$ powders [1]. A study of sintering kinetics and shrinkage behaviour of the powder compacts is essential for fabrication of single-phase high-density crack-free sintered bodies with good superconducting properties. Evaporation loss of barium and copper during sintering of pellets and films, which leads to non-stoichiometry, have been reported [2, 3]. Further, in this system, the nature of the grain boundary has a large effect on the superconducting properties of the sample (weak-link behaviour of the grain boundary) owing to its inherent non-stoichiometry [4]. Hence optimization of sintering parameters/conditions is important for reduction of processing time and attainment of optimum properties.

The sintering behaviour of homogeneous $YBa_2Cu_3O_x$ powders in an ambient atmosphere is reported here. The influence of the presence of unreacted phases was also investigated.

2. Experimental procedure

Y–Ba–Cu-oxide powder with nominal composition $YBa_2Cu_3O_x$ was prepared through the pyrophoric route [5] using Y_2O_3 (99.99% pure from Indian Rare Earth Limited), $Ba(NO_3)_2$ and $Cu(NO_3)_2 \cdot 3H_2O$ (both 99% pure from Merck, India) powders. The particle size of ultrasonically dispersed powders (calcined at 1203 K) was found to be less than 50 nm (Fig. 1) by TEM (Phillips CM 12). The powders being very fine, are highly reactive with CO_2 and water vapour present in air and, as a result, if left in the open atmosphere, hydroxides and carbonates of the constituent cations are formed. The pyrophorically generated powders, if processed immediately after synthesis, yield $YBa_2Cu_3O_x$ at calcination temperatures as low as 1023 K. In this work, two types of powder were used: pyrophorically generated powder (A) which has been calcined at 1023 K, to obtain a homogeneous mass of $YBa_2Cu_3O_x$ as evidenced by X-ray diffraction analysis, and pyrophorically generated powder (B) which had been left open to the atmosphere to allow formation of hydroxides and carbonates of Y^{3+}, Ba^{2+} and Cu^{2+} on the surface of the grains. Equal amounts of the powders (≈ 6.7 g) A and B were pressed uniaxially, without any binder, into cylindrical pellets (diameter = 2.45 cm) under a pressure of 12.4 MPa. The green densities of the pellets were 3.75 and 3.50 g cm^{-3} for pellets A (from powder A) and pellets B (from powder B), respectively. The green pellets were cut into rectangular pieces ($\approx 7.5 \times 5 \times 3.8$ mm^3 for A and $\approx 7.5 \times 5 \times 4.0$ mm^3 for B) for thermomechanical analysis (TMA) and stored in a vacuum desiccator to avoid atmospheric degradation. Detailed thermal (differential thermal analysis, thermogravimetry and TMA) structural and microstructural analysis of the pellets were performed to determine the sintering behaviour.

A Shimadzu DT 30 thermal analyser system with quartz dilatometer (TMA-30) was used for the sintering study. The change in length could be measured with an accuracy of $\pm$ 5 μm and temperature of

0022–2461

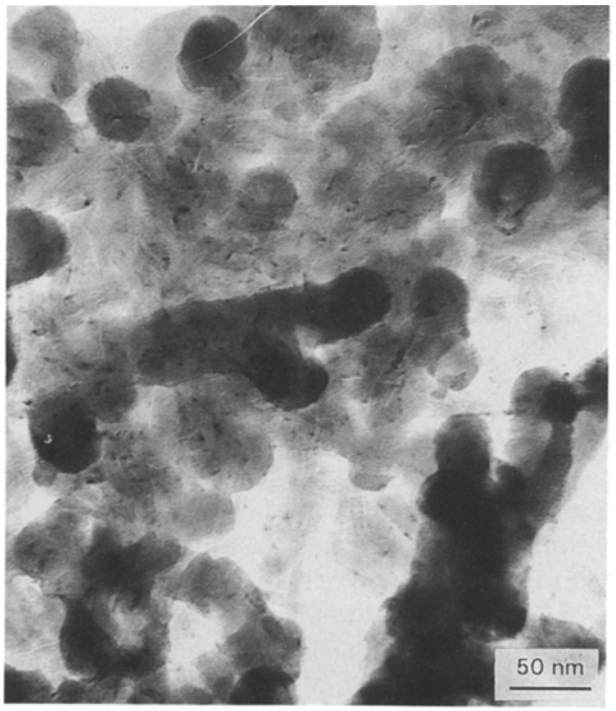

Figure 1 Transmission electron micrograph of pyrophorically generated $YBa_2Cu_3O_x$ powder calcined at 1173 K.

the sample could be controlled within $\pm$ 1 K. Platinum plates, 0.05 mm thick, were used as a barrier between the sample and quartz sensor rod on top and the sample holder at the bottom to avoid interaction between the quartz and YBCO. Isothermal sintering was carried out for all the samples for 1 h at a heating rate of 10 K min^{-1}. The samples had a smaller height compared to the base dimensions. The push rod rested gently on the sample with a load of 138 Pa in order to discount the possibility of any creep deformation. Pellets prepared from powder A were sintered at isothermal temperatures ranging from 1173–1271 K for 1 h in static air, flowing argon and oxygen (50 cm^3 min^{-1}). Argon and oxygen were of commercial grade purity. Pellets prepared from powder B were sintered for 1 h at temperatures varying from 1073–1273 K in static air. The apparent densities of all the samples studied were measured using Archimedes' principle. Differential thermal analysis (DTA) and thermogravimetry (TG) measurements were also performed on both the powders A and B.

X-ray diffraction (XRD), SEM and optical microscopy of the samples at various stages of sintering were performed. A Phillips PW 1840 system with nickel-filtered CuK_α radiation was used for XRD analysis. Gold-coated fractured surfaces of the samples were analysed by SEM (CAM SCAN). Sintered samples were oxygenated at 773 K for 20 h and cooled at the rate of 60 K h^{-1} to room temperature. A.c. susceptibility of the samples was measured at a field of 1 Oe and frequency of 80 Hz from 100–15 K. The resistivity and critical current density of the samples were also measured.

3. Results and discussion

The densification parameter, α ($\delta L/L_0$), is time dependent because of the systematic decrease of the porosity of the compact with sintering time. Experimentally, it is convenient to measure the $\delta L/L_0$ continuously with time using dilatometry. α can be expressed as a function of sintering variables [6, 7].

$$\alpha^{1/n} = K' e^{-Q/(RT)} t \quad (1)$$

where Q is the activation energy for the rate-governing step in sintering, n the sintering kinetic parameter, R the gas constant, t the time, T the temperature (K), and K' is a constant. From Equation 1 we have

$$(1/n)\ln\alpha = \ln K' - Q/(RT) + \ln t \quad (2)$$

The values of n, obtained from the slopes of straight lines obtained by plotting $\ln\alpha$ versus $\ln t$ at various temperatures could be subsequently used for the calculation of Q from Equation 2.

Fig. 2 shows typical sintering curves where change of length, δL, and temperature are plotted as a function of time. The sintering curve can be divided into three regions, heating zone (AB), isothermal region (BC) and cooling zone (CD). The samples showed no change other than thermal expansion and contraction during heating or cooling and showed a time-dependent shrinkage during isothermal holding. At higher temperatures, however, the shrinkage began even before the final temperature could be reached. The error in calculations due to shrinkage (while heating) of the specimen prior to the isothermal sintering could be eliminated by converting the time required for the total shrinkage before achieving the isothermal state, to the time required at that isothermal temperature using Equation 2. An iterative method was used for the final estimation of n and Q.

Figs 3–5 show the variation of the sintering parameter, α, with iterated time (min), for compacts made from powder A under different atmospheres. The logarithmic time dependence of the isothermal shrinkage has been plotted in Figs 6–8. The slopes of these curves yield a value of n between 0.45 and 0.5. The logarithmic rate of change of length under different ambient atmospheres has been plotted as a function of the inverse of absolute temperature in Fig. 9. The activation energy for sintering, calculated from the slopes has been found to be 1218 kJ mol^{-1} in argon,

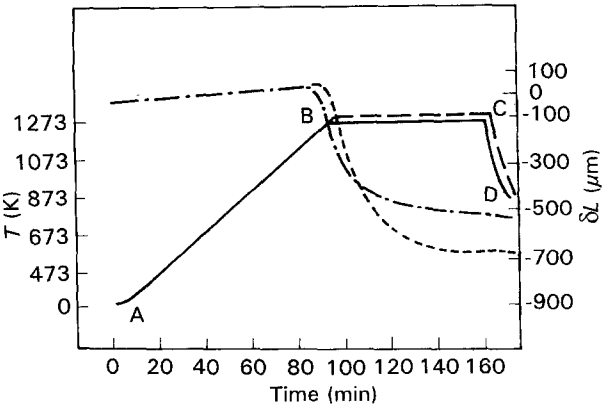

Figure 2 Variation of the change of (—·—, - - -) length, δL, and (—, – –) temperature of a sample as a function of time for (- - -, – –) pellet A and (—·—, —) pellet B.

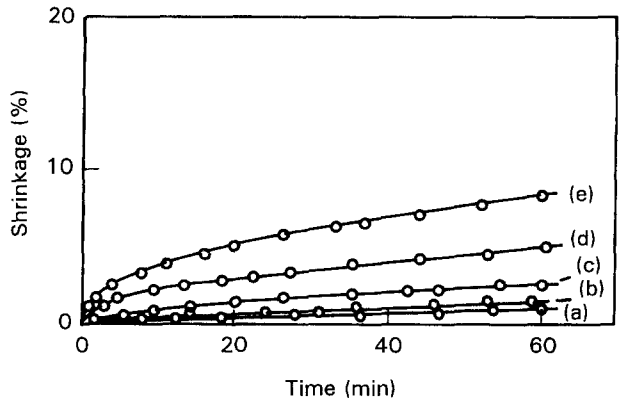

Figure 3 Variation of shrinkage with sintering time for pellet A sintered in flowing oxygen (50 $cm^3 min^{-1}$) at (a) 1225 K, (b) 1233 K, (c) 1243 K, (d) 1255 K and (e) 1261 K.

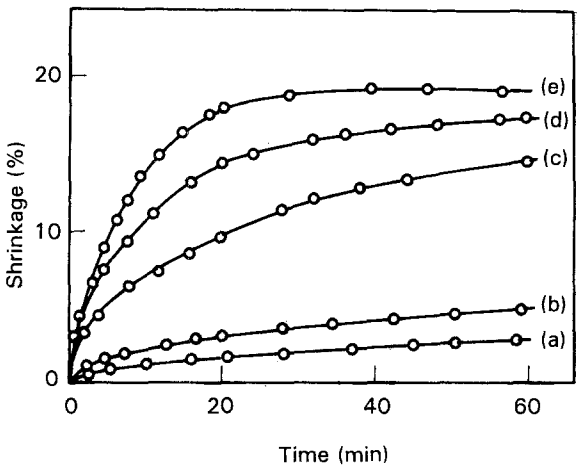

Figure 4 Variation of shrinkage with sintering time for pellet A sintered in static air at (a) 1203 K, (b) 1220 K, (c) 1240 K, (d) 1247 K and (e) 1251 K.

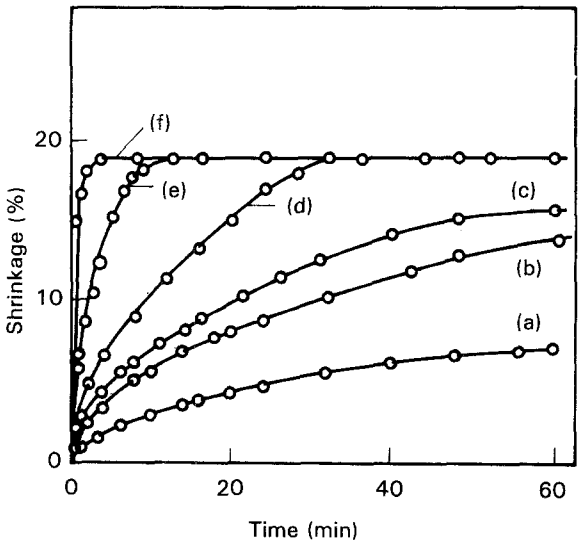

Figure 5 Variation of shrinkage with sintering time for pellet A sintered in flowing argon (50 $cm^3 min^{-1}$) at (a) 1196 K, (b) 1207 K, (c) 1211 K, (d) 1218 K, (e) 1223 K and (f) 1238 K.

1593 $kJ mol^{-1}$ in air and 2142 $kJ mol^{-1}$ in a pure oxygen atmosphere.

The variation of α with the sintering time (Figs 3–5) indicates that the rate of shrinkage is environmentally

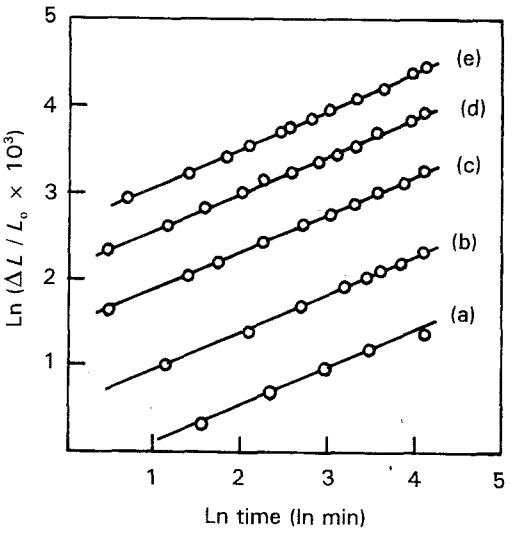

Figure 6 Logarithmic time dependence of shrinkage for pellet A sintered in flowing oxygen (50 $cm^3 min^{-1}$) at (a) 1214 K, (b) 1233 K, (c) 1243 K, (d) 1255 K and (e) 1261 K.

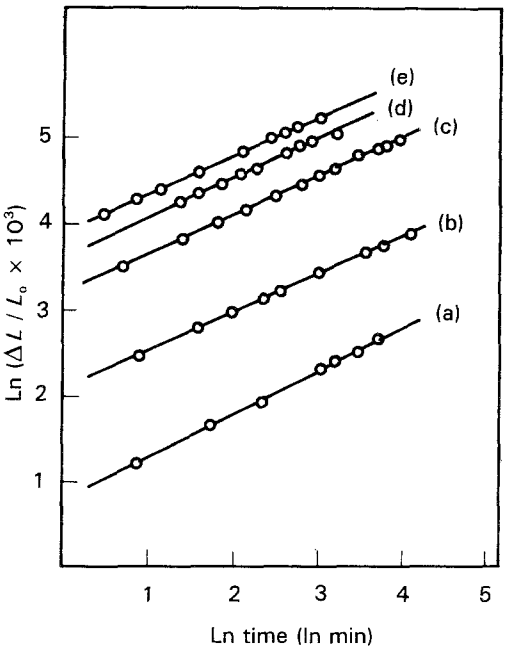

Figure 7 Logarithmic time dependence of shrinkage for pellet A sintered in static air at (a) 1203 K, (b) 1220 K, (c) 1240 K, (d) 1247 K and (e) 1251 K.

dependent. As the partial pressure of oxygen in the sintering atmosphere is increased, the sintering parameter, α, decreases. The rate of densification with temperature also shows a similar behaviour (Fig. 10). The reported lattice self-diffusion activation energies for diffusion of metal ions in Y–Ba–Cu-oxide compound are Y^{3+} = 433.5 $kJ mol^{-1}$, Ba^{2+} = 338.6 $kJ mol^{-1}$ and Cu^{2+} = 250.8 $kJ mol^{-1}$ [8] and that of oxygen = 250.8 $kJ mol^{-1}$ [9] are much lower than the apparent activation energies observed for sintering which indicates that the sintering phenomenon in this system may not be due to a single diffusion-step controlled process.

The enhanced sintering under low partial pressure of oxygen (0.004 bar in argon, and air) atmosphere may be due to the following reasons: (a) creation of

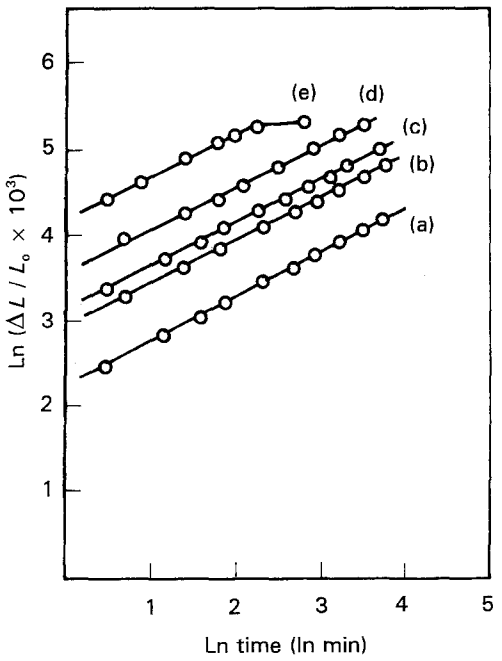

Figure 8 Logarithmic time dependence of shrinkage for pellet A sintered in flowing argon (50 $cm^3 min^{-1}$) at (a) 1196 K, (b) 1207 K, (c) 1211 K, (d) 1218 K and (e) 1223 K.

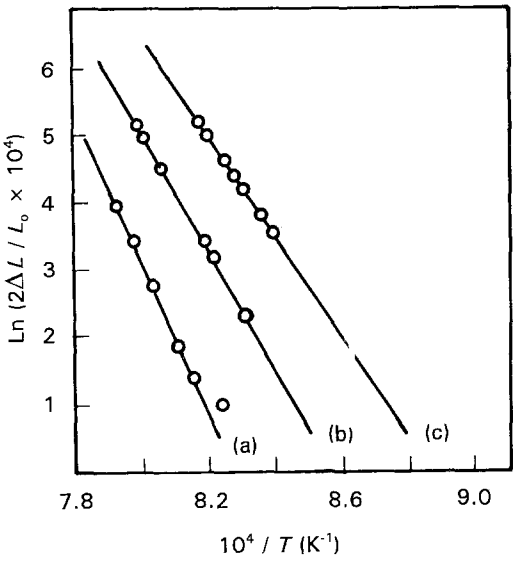

Figure 9 Plots for the estimate of activation energies for pellet A sintered in (a) flowing oxygen (50 $cm^3 min^{-1}$), (b) static air and (c) flowing argon (50 $cm^3 min^{-1}$).

oxygen vacancies which lead to enhanced diffusion and hence sintering, and (b) formation of small amounts of liquid phase at the grain boundaries where the grains are pressed against each other [10]. However, the liquid phase, if formed, is very small because the polarized light optical micrographs of the polished sections do not show the presence of any optically active phase other than the 123 phase in significant amounts. Scanning electron micrographs (Fig. 11a–d) of the fractured surface show the grain growth associated with densification under the three ambient atmospheres. No phase separation was observed for samples sintered under argon but platelet-type grain

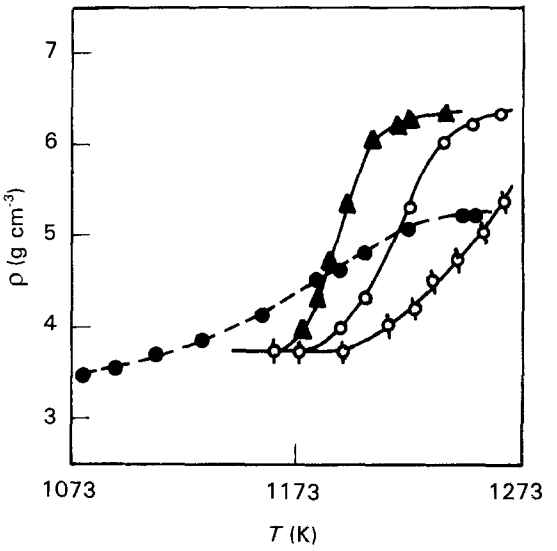

Figure 10 Variation of the apparent density with temperature for a soaking time of 1 h for pellet A sintered in (ϕ) oxygen, (○) air and (▲) argon, and (●) for pellet B sintered in air.

growth was easily observed. The porosity also can be seen to decrease with increasing grain growth.

Thermogravimetric analysis of powder A did not indicate any weight loss in the temperature range 1073–1253 K. Differential thermal analysis shows one endothermic peak at 1050 K which is due to phase transformation of 123. Although XRD of the samples sintered under different atmospheres shows some change in the diffraction pattern (Fig. 12), the diffraction peaks are due to the 123 phase only, which suggests the absence of any peritectic reaction in the sample.

A.c. susceptibility measurements on sintered samples which had been subsequently oxygenated at 773 K under flowing oxygen for 20 h, show that the transition width is sharper for the samples sintered in argon compared to those sintered in air or oxygen (Fig. 13). It was observed from the resistivity and critical current density (near $T = T_c$) measurement that there are more weak links in oxygen-sintered samples compared to the samples sintered in an argon atmosphere. The variation of critical current density with temperature indicates that the nature of the weak links changes from S–I–S type to S–N–S type as the partial pressure of oxygen increases during sintering.

A typical variation of α with time for the pellets B which start sintering from 1073 K, is given in Fig. 14. The plot of $\ln\alpha$ versus $\ln t$ shows two stages of sintering (Fig. 15), one between 1073 and 1173 K ($n = 0.5$) and the other between 1173 and 1273 K ($n = 0.22$) with corresponding activation energies of 627 and 383.7 kJ mol^{-1} (Fig. 16). The densification curve (Fig. 10) shows that a maximum of 85% theoretical density is achieved. Phase formation starts at 1173 K with the decomposition of $BaCO_3$ as confirmed from TG and DTA (Fig. 17) and XRD (Fig. 18). DTA analysis of the powder B shows two endothermic peaks, one at 1073 K due to phase transformation of $BaCO_3$ [11] and another peak with onset at 1173 K due to decomposition of $BaCO_3$, as seen from TGA. However, there was no evidence for

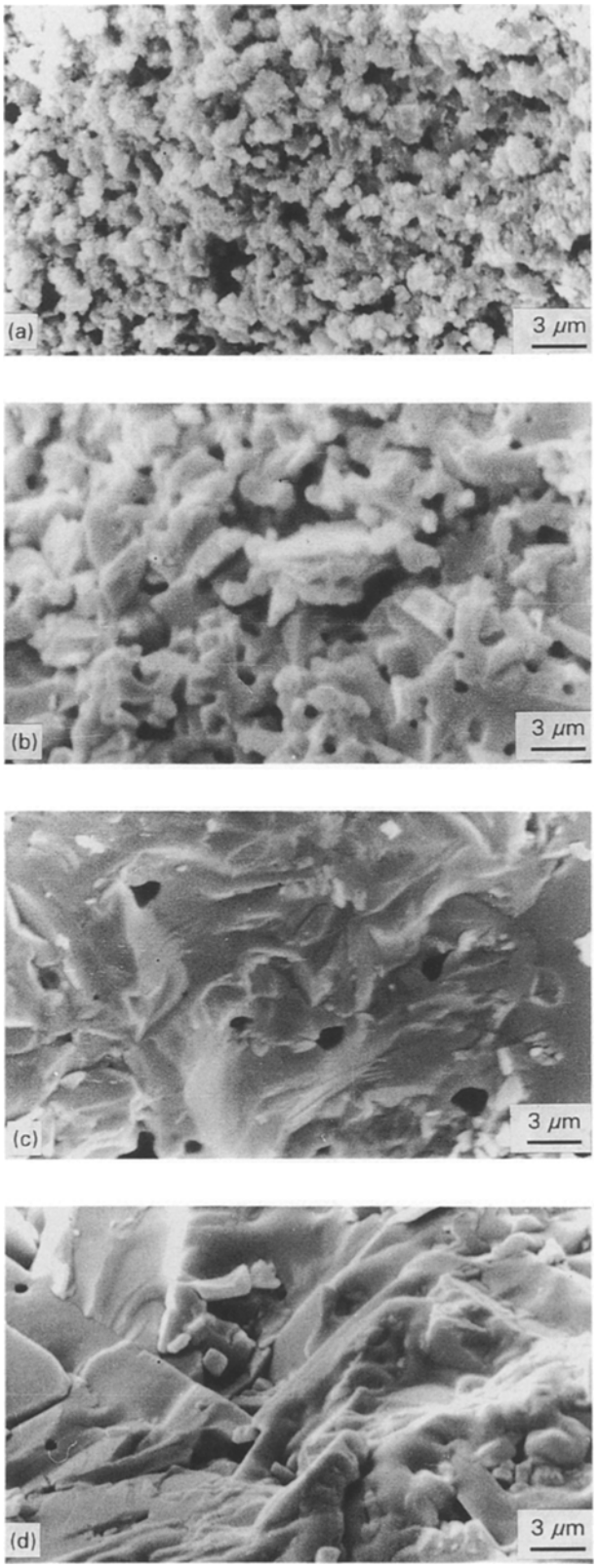

Figure 11 Scanning electron micrographs of pellets A: (a) green pellet, (b) sintered in oxygen at 1264 K for 1 h, (c) sintered in air at 1263 K for 1 h, and (d) sintered in argon at 1223 K for 1 h.

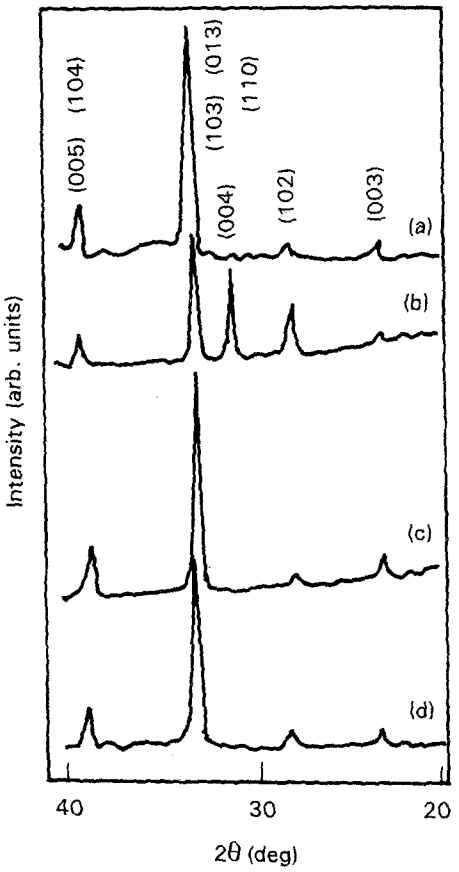

Figure 12 XRD patterns of pellets from powder A: (a) green pellet, and pellets sintered at 1233 K for 1 h under (b) oxygen, (c) air and (d) argon atmospheres.

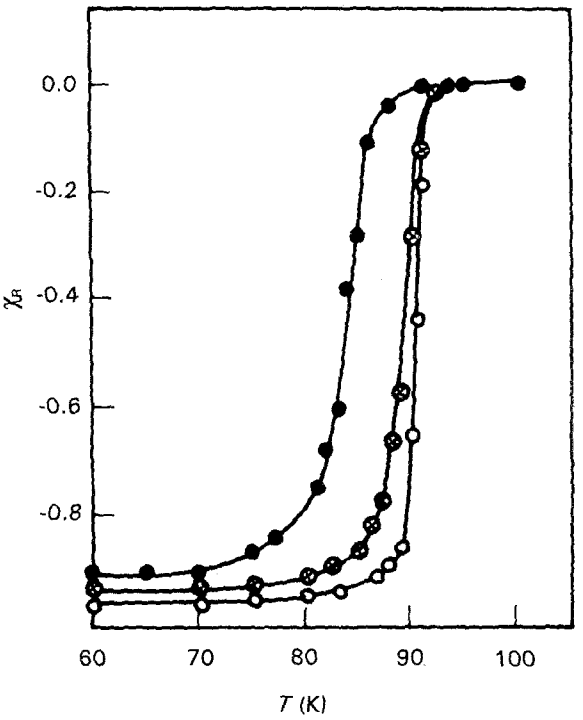

Figure 13 Variation of χ_R, with temperature of the pellet A sintered for 1 h at 1233 K in (●) oxygen, (⊗) air and (○) argon.

the existence of endothermic peak at 1233 K, which indicates the absence of $BaCuO_2$ in the reacting mass. The densification of the compacts, made from powder B, in the range 1073–1173 K in air could be due to the coalescence of the grains through surface diffusion and vapour-phase transport to the neck without any chemical transformation. The enhanced rate of densification observed above 1173 K is possibly due to the formation of 123 phase. The scanning electron micrographs (Fig. 19a–c) of samples B show that the grain growth is inhibited compared to samples A

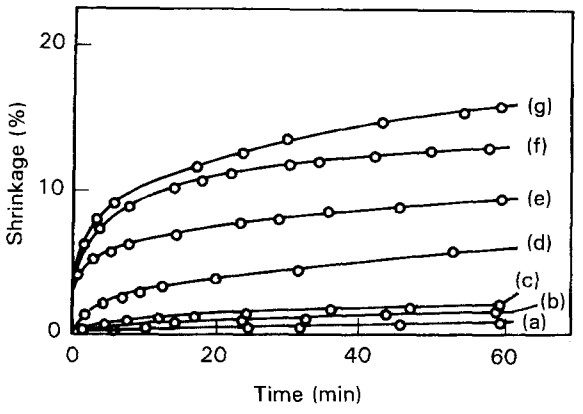

Figure 14 Variation of shrinkage with sintering time for pellet B sintered in static air at (a) 1078 K, (b) 1104 K, (c) 1120 K, (d) 1158 K, (e) 1173 K, (f) 1208 K and (g) 1238 K.

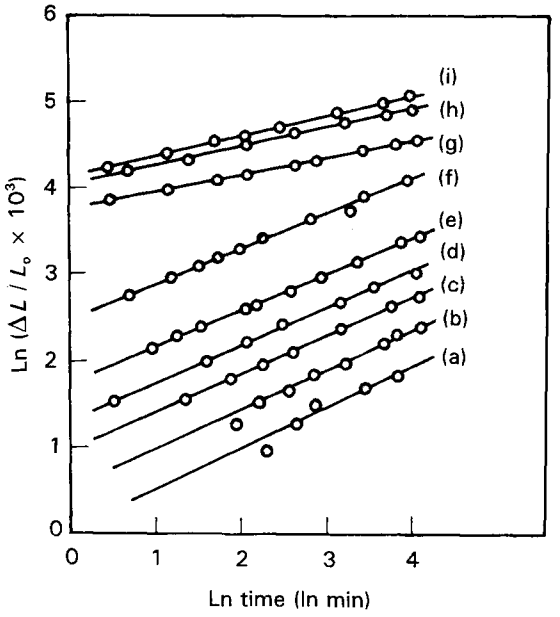

Figure 15 Logarithmic time dependence of shrinkage of pellet B sintered in static air at (a) 1078 K, (b) 1093 K, (c) 1104 K, (d) 1120 K, (e) 1130 K, (f) 1158 K, (g) 1173 K, (h) 1208 K and (i) 1238 K.

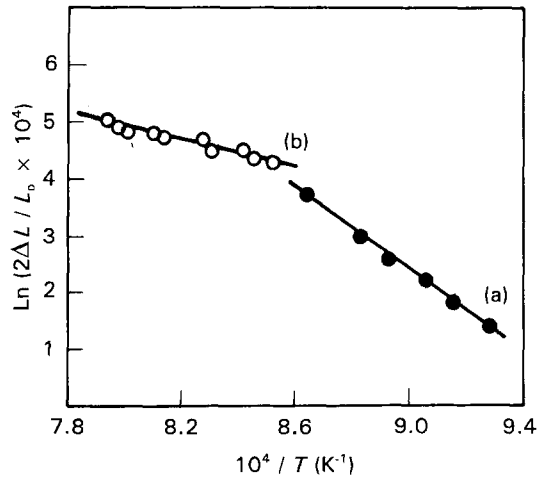

Figure 16 Plots for the estimation of activation energies for pellet B sintered in static air at (a) 1073–1173 K and (b) 1173–1273 K.

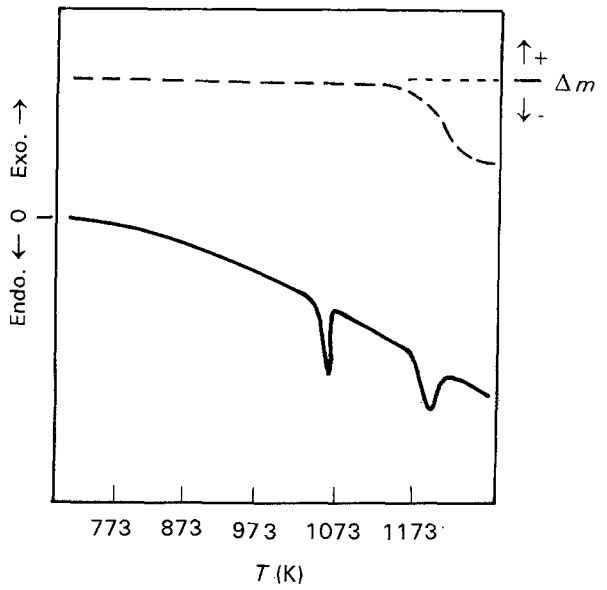

Figure 17 TG and DTA of powder B in static air.

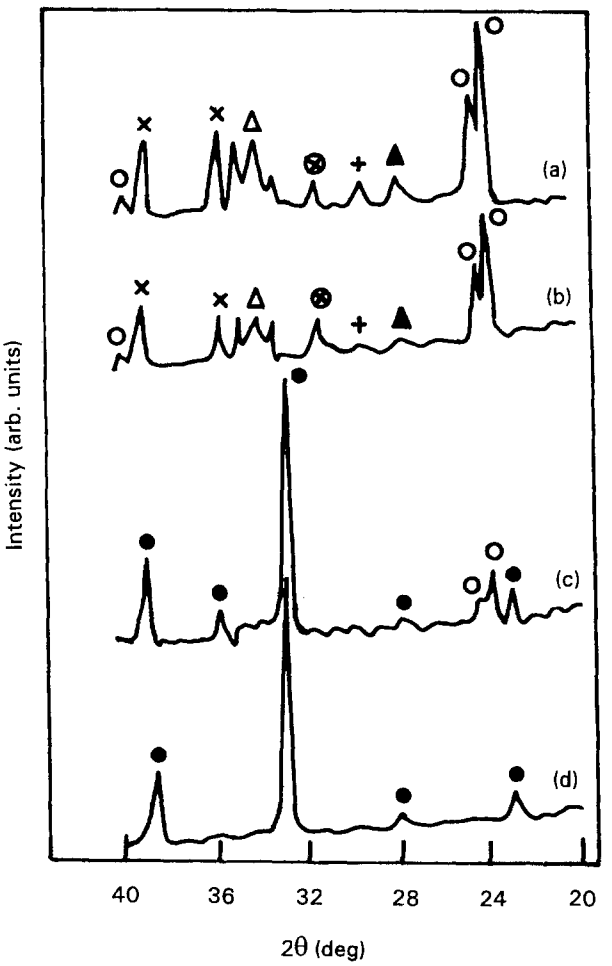

Figure 18 XRD patterns of pellet B sintered in static air for 1 h at (a) 1078 K, (b) 1132 K, (c) 1173 K and (d) 1233 K. (●) $YBa_2Cu_3O_x$, (○) $BaCO_3$, (×) CuO, (▲) $Ba(OH)_2$, (+) Y_2O_3, (⊗) Y_2BaCuO_5 and (△) $CuYO_2$.

(Fig. 11). The presence of inhomogeneity and pores inhibits the grain growth.

In the present investigation, the presence of chemical inhomogeneity (sample B) has consistently given rise to lower activation energies for sintering. While

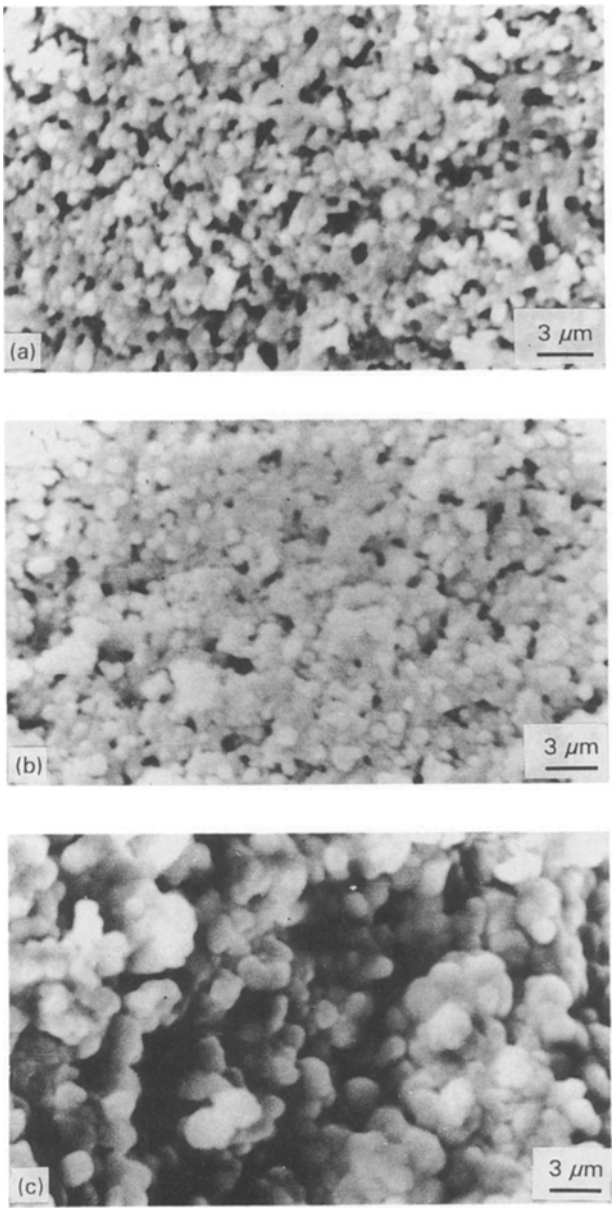

Figure 19 Scanning electron micrographs of pellet B sintered for 1 h in static air at (a) 1158 K, (b) 1173 K and (c) 1253 K.

the complete phase diagram for the Y–Ba–Cu-oxide system has not yet been fully investigated, Roth *et al.* [12] point out the existence of a series of low-melting phases in the system. Although thermal analysis of sample B could not reveal any such melting in the range of TMA investigation, the possibility of the existence of phases of high defect concentration (solid to liquid transition) in sample B cannot be ruled out. The presence of such phases may be responsible for the faster rate and defect-assisted sintering mechanism (lower activation energies).

4. Conclusions

1. A detailed study on the sintering behaviour and the concomitant structural and microstructural changes in the Y–Ba–Cu-oxide system has been carried out.

2. The partial pressure of oxygen during sintering has been found to have a profound influence on the densification behaviour. Samples sinter several times faster and at lower temperatures under an argon atmosphere than under air or oxygen, leading to a large reduction of processing time and temperature.

3. Pellets sintered under argon followed by oxygenation at 773 K for 20 h have sharper superconducting transition than those processed in air or oxygen.

4. The presence of unreacted constituents causes a decrease in the sintering rates and restricts grain growth in sintered samples.

References

1. N. YANG, C. L. YANG and P. T. WU, *J. Mater. Sci.* **27** (1992) 1978.
2. T. SATA, K. SAKAI and S. TASHIRO, *J. Amer. Ceram. Soc.* **74** (1991) 1445.
3. S. K. MISHRA, L. C. PATHAK, M. V. H. RAO, D. BHATTACHARYA and K. L. CHOPRA, *Ind. J. Pure Appl. Phys.* **30** (1992) 685.
4. S. E. BABCOCK and D. C. LARBALESTIER, *Appl. Phys. Lett.* **55** (1990) 393.
5. D. BHATTACHARYA, L. C. PATHAK, S. K. MISHRA, D. SEN and K. L. CHOPRA, *ibid.* **57** (1990) 2145.
6. L. LEVIN, S. F. DIRNFIELD and D. SHWAM, *Powder Met. Int.* **12** (1980) 26.
7. R. M. GERMAN and Z. A. MUNIR, *Powder Met.* **3** (1977) 145.
8. J. L. ROUTBORT, S. J. ROTHMAN, N. CHEN, J. N. MUNDY and J. E. BAKER, *Phys. Rev. B* **43** (1991) 5489.
9. T. NAGARAJAN, V. SRIDHARAN, S. SIVASANKARAN, D. K. BISWAS and K. NANDHINI, *Ind. J. Pure Appl. Phys.* **30** (1992) 609.
10. K. W. LAY and G. M. RENLUND, *J. Amer. Ceram. Soc.* **72** (1990) 1208.
11. R. WEAST and M. J. AUSTLE, "CRC Handbook of Chemistry and Physics", 60th Edn (CRC Press, Cleveland, OH, 1980) p. B58.
12. R. S. ROTH, K. L. DAVIS and J. R. DENNIS, *Adv. Ceram. Mater.* **2** Special issue (1987) 303.

Received 16 February
and accepted 12 November 1993